Privacy Preserving Contraband Detection Using a Millimeter-Wave Dynamic Antenna Array

Daniel Chen, *Graduate Student Member, IEEE*, and Jeffrey A. Nanzer, *Senior Member, IEEE*

***Abstract*— We present a privacy preserving technique for contraband detection using a real-time 75 GHz rotational dynamic antenna array that samples only a reduced set of Fourier-domain information to prevent image reconstruction of the screened subject. Complex objects such as handguns have sharp edges that correspond to sharp spatial frequency features in the Fourier domain. These features are dependent on the orientation of the object and manifest at millimeter-wave frequencies through conditions such as being concealed under clothing. The technique combines a dynamically rotated active interferometer and simple arithmetic feature extraction approach supporting a threshold-based classifier to identify when a handgun is concealed under clothing. The active interferometer technique utilizes noise transmitters to illuminate the test subject to produce thermal-like radiation, enabling Fourier-domain signal sampling, while the rotational dynamics support sampling that spans a circle in the 2-D Fourier domain to retrieve sharp-edge responses induced by concealed objects. We experimentally demonstrate the detection of concealed objects under clothing in a laboratory environment using a 75 GHz dynamic antenna array based on simple heuristic features extracted from statistics of the measured responses. The classifier is evaluated based on processing one or more subsequent measurements, showing a classification accuracy of 0.908 and $F1$-score of 0.916 using four consecutive measurements.**

***Index Terms*— Contraband detection, dynamic antenna arrays, millimeter-wave interferometer, noise radar.**

I. Introduction

MILLIMETER-WAVE systems are beneficial in imaging and sensing applications because the wavelengths are sufficiently short to support adequate image resolution while also being long enough for sufficient propagation through garments, fog, smoke, and other obscurants with negligible attenuation [1], [2]. Interferometer-based imaging systems measure scene information in the Fourier domain and have been adopted for their ability to recover high-resolution imagery using only a fraction of the physical aperture area when compared to implementations using focal plane arrays and/or those that use electronically- or mechanically-steered antennas [3], [4]. Concealed contraband detection via imagery typically relies on rigorous classification processes to identify objects [5]. However, such an approach relies on fully reconstructed imagery, which can be expensive to obtain due to the need for additional hardware, such as many receiving antennas, and extensive computational resources. In contrast, prior work has shown that objects with sharp edges manifest identifiable artifacts in the Fourier domain and present the opportunity for direct object detection and classification without relying on imagery, with the potential for significant reductions in the cost of the overall sensing system [6]. However, the practical use of the technique in detecting and classifying objects has not been investigated. In particular, object orientation affects the backscattered signals, which may yield wide variations in the measured Fourier-domain information, adversely impacting classification.

In this work, we present an approach for privacy-preserving contraband detection using a 75 GHz dynamic antenna array and a simple classifier. Spatial Fourier-domain samples are captured by a rotating dynamic antenna array and simple arithmetic operations are used to compute threshold values where the appearance of concealed contraband is identified regardless of its placement and orientation with respect to the sensing array. Other work has focused on obtaining specific Fourier-domain responses that are orthogonal to the sharp-edge direction [6]. However, such signatures are only recoverable when the object is specifically placed. In this work, we incorporate a simple classifier on a significantly larger data set considering a more realistic replication of a common contraband object while allowing variation on the placement of the object and the background testing subject to imitate practical concealed contraband scenarios. We demonstrate the separability of Fourier-domain features of contraband and non-contraband scenes, and threshold-based classification with an accuracy of 0.908 and $F1$-score of 0.916.

II. Millimeter-Wave Interferometric Dynamic Antenna Array

The viability of active millimeter-wave interferometric sensing over traditional passive interferometric systems that solely rely on low-power thermal radiation has been shown in recent years by using noise transmission to mimic spatio-temporal properties of thermal radiation and thus improve the received signal-to-noise ratio compared to passive systems [7]. The interferometric measurement takes place in the Fourier domain, which is often referred to as the *visibility* $V(u, v)$, where u and v represent the two spatial frequency dimensions. When the signals scattered off the scene are spatio-temporally incoherent, a condition supported by the transmission of noise signals, the visibility is related to the scene intensity $I(\alpha, \beta)$ via the 2-D Fourier transformation given by [8], [9]

$$V(u, v) = \iint_{-\infty}^{+\infty} I(\alpha, \beta) e^{j2\pi(u\alpha+v\beta)} d\alpha d\beta \tag{1}$$

Manuscript received 24 February 2023; accepted 29 March 2023. Date of publication 28 April 2023; date of current version 7 June 2023. This work was supported in part by the National Science Foundation under Grant 1751655. *(Corresponding author: Jeffrey A. Nanzer.)*

The authors are with the Department of Electrical and Computer Engineering, Michigan State University, East Lansing, MI 48824 USA (e-mail: chendan7@msu.edu; nanzer@msu.edu).

This article was presented at the IEEE MTT-S International Microwave Symposium (IMS 2023), San Diego, CA, USA, June 11–16, 2023.

Color versions of one or more figures in this letter are available at https://doi.org/10.1109/LMWT.2023.3267678.

Digital Object Identifier 10.1109/LMWT.2023.3267678

2771-957X © 2023 IEEE. Personal use is permitted, but republication/redistribution requires IEEE permission.
See https://www.ieee.org/publications/rights/index.html for more information.

Authorized licensed use limited to: Michigan State University. Downloaded on June 27,2024 at 04:23:30 UTC from IEEE Xplore. Restrictions apply.

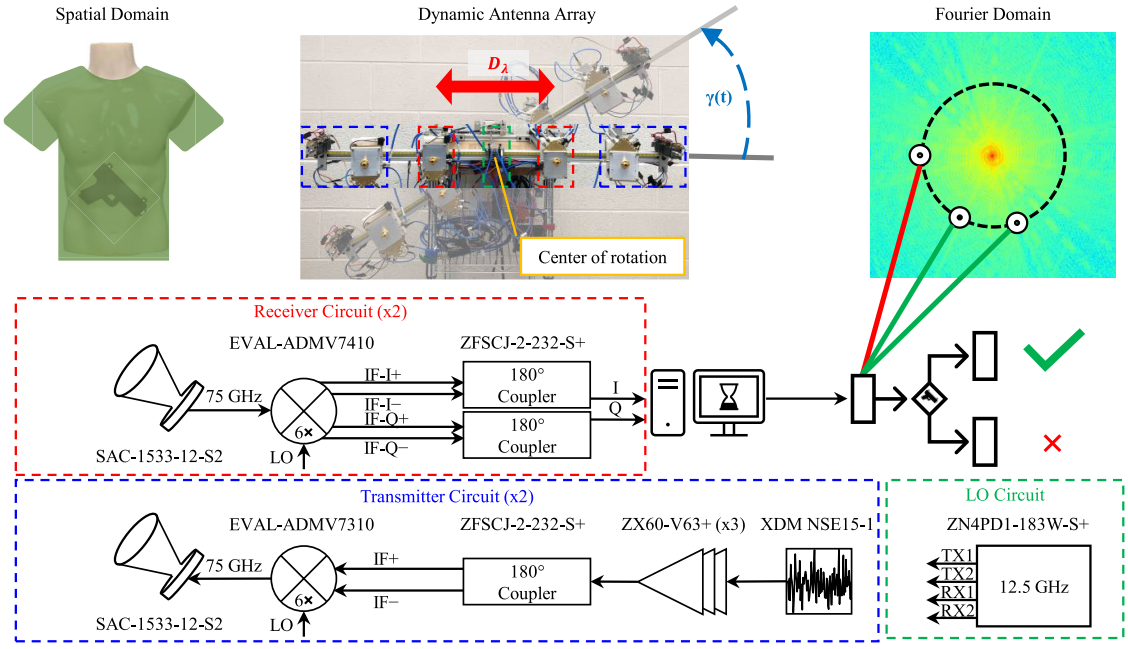

Fig. 1. Concept diagram and system architecture of the experimental millimeter-wave dynamic antenna array which comprises two transmitters (blue dashed box), two receivers (red dashed box), and a local oscillator (LO) circuit (green dashed box). The noise transmitters enable Fourier-domain sampling by satisfying spatio-temporal incoherence condition. The two received signals at each sampled angle are cross-correlated with the obtained visibility samples defined by the antenna baseline D_λ. As the dynamic antenna array rotates at angle $\gamma(t)$, the corresponding Fourier-domain sample rotates in the uv-space, thus additional Fourier-domain information can be obtained. The signals are sent to a classifier to determine whether a specific contraband, e.g., a handgun, is concealed by the screened subject. LO: local oscillator. IF: intermediate frequency. TX: transmitter. RX: receiver.

where $\alpha = \sin\theta\cos\phi$ and $\beta = \sin\theta\sin\phi$ are the direction cosines. For a given two-element interferometer, the antenna arrangement determines the subset of available visibility samples that can be measured via the sampling function

$$S(u, v) = \sum_{n=1}^{N}\sum_{m=1}^{M}\delta(u - u_n)\delta(v - v_m) \tag{2}$$

where $N \cdot M$ is the maximum number of unique spatial frequency samples that can be measured and $\delta(\cdot)$ represents the Dirac delta function. The sampled visibility is thus the product of (1) and (2). Imaging systems reconstruct the scene intensity via 2-D inverse Fourier transform of the sampled visibility; in this work, we operate directly on the sampled visibility. Specific u and v samples are defined by the configuration of receiving antennas based on their spatial placement x and y and the system wavelength $\lambda = c/f$ such that $u = D_x/\lambda$ rad^{-1} and $v = D_y/\lambda$ rad^{-1}, where D_x and D_y are the physical separation of the receiving antennas in the x and y dimensions.

While traditional millimeter-wave interferometric systems fix the antennas spatially, the sampling function can be dynamically synthesized and improved by allowing the receiving antennas to move within the aperture plane. One particular dynamic approach is the rotation of an antenna pair with respect to its centroid, in which the resulting sampling function has a ring shape that covers various spatial frequencies at different angles [6]. Using this approach, the sampled visibility can be represented as a collection of measurements by

$$\mathbb{S} = S(u_k, v_k) \quad \forall k = [0, K-1] \tag{3}$$

where u_k and v_k are the uv-samples defined by the receiver separation normalized to the wavelength D_λ and the K discrete rotational angles $\gamma(k)$ over 180° as $u_k = D_\lambda \sin\gamma(k)$ and $v_k = D_\lambda \cos\gamma(k)$, respectively. The system response is thus a vector of the Fourier-domain samples obtained as a function of angle.

Based on this principle, we implemented a two-element rotationally dynamic interferometric receiver, as shown in Fig. 1. The dynamic antenna array operated at 75 GHz and was based on that of [6]. The system comprises two noise transmitting sources and two receivers. Each of the two transmitters includes a noise source with a bandwidth of 10–1600 MHz (RF-Gadgets XDM NSE15-1), three cascaded baseband amplifiers (Mini-Circuits ZX60-V63+), a 180° coupler (Mini-Circuits ZFSCJ-2-232-S+), an upconverter (Analog Devices EVAL-ADMV7310), and a 15 dBi linearly polarized conical horn antenna (Eravant SAC-1533-12-S2). Each of the two receivers includes an identical 15 dBi conical horn antenna, a downconverter (Analog Devices EVAL-ADMV7310), and two 180° coupler (Mini-Circuits ZFSCJ-2-232-S+).

III. Experiment and Analysis

Experiments were conducted to determine the separability of the Fourier-domain responses of scenes with and without contraband present. The experiment consisted of 160 independent measurements equally grouped into two general classes as shown in Fig. 2: a clothed fiberglass mannequin facing toward the dynamic antenna array with and without a gun-shape target of dimension 164 × 235 mm concealed underneath the clothing. Between each successive measurement, the mannequin was removed and replaced to mimic the uncertainties of a practical test subject's relative orientation to the dynamic antenna array due to breathing and/or torso movements. Similarly, the gun-shaped target was randomly placed beneath the clothing with its barrel pointing at varying directions. The mannequin with and without the gun-shape target was approximately 1.83 m from the dynamic antenna array and was backed by walls of radio frequency absorbers. The two receivers of the array were 77λ apart at 75 GHz and rotated over a 180°

Authorized licensed use limited to: Michigan State University. Downloaded on June 27,2024 at 04:23:30 UTC from IEEE Xplore. Restrictions apply.

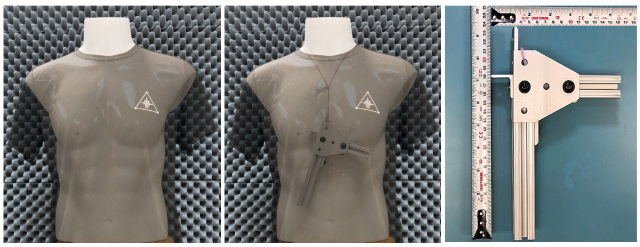

Fig. 2. From left to right: Front of a clothed mannequin (t-shirt shown transparent to show mannequin); front of a clothed mannequin with a concealed gun-shape target; the gun-shape target of dimension 164 × 235 mm.

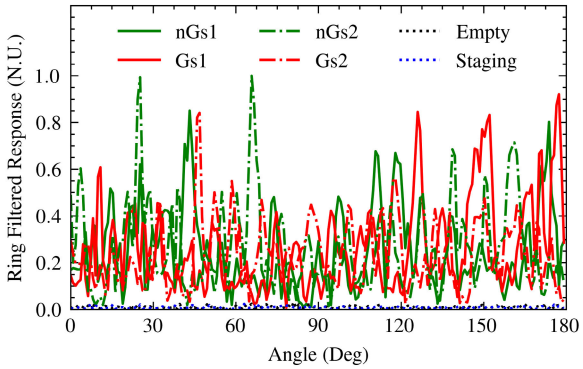

Fig. 3. Six examples of the ring filtered responses (3) using the dynamic antenna array at $D_\lambda = 77\lambda$. The black and blue dash lines are the responses of empty scene and absorbing staging materials, respectively. The solid green/red and dash-dot green/red lines show how varying mannequin placements and/or gun-shape target can affect the measured responses. Gs: gun-shape. nGs: non-Gun-shape. N.U.: normalized unit.

rotational span at every 0.9° (equivalent to the motor encoder resolution) for all measurements. The two received signals at all 200 angles, tracing out a ring-shape sampling function, each with dwelling time of $\tau = 1$ ms, were then cross-correlated to recover the Fourier-domain information and form the ring filtered response $\mathbb{S}$. Examples of ring-filtered responses are shown in Fig. 3 where the black and blue dashed lines represent the responses of an empty scene and a scene with only the absorbing staging materials, and the green/red pair in dash and dash-dot lines are two sets of data from the scene with and without the gun shape, respectively. It is clear that the two classes are difficult to differentiate based solely on the sampled output in the Fourier domain from the dynamic antenna array.

To overcome this challenge, we investigated a multi-feature classification approach using 11 heuristically defined features, each of which was a different algorithmic process on the sampled Fourier-domain data $\mathbb{S}$. The 11 features were: mean, median, maximum, standard deviation, variance, difference between maximum and minimum, difference between the maximum and mean, difference between maximum and median, difference between mean and minimum, difference between median and minimum, and difference between the median and mean. The magnitude of the 11-feature space vector was computed for each measurement and normalized to all measurements. As seen in Fig. 4, the two distributions display significant differences despite the similarities between the two classes of $\mathbb{S}$ seen in Fig. 3. The responses with no target are concentrated below a normalized feature vector magnitude of 0.2, while the responses with a target spread over a wider range. This difference in the distribution points to a threshold value of the normalized feature vector magnitude of approximately 0.2.

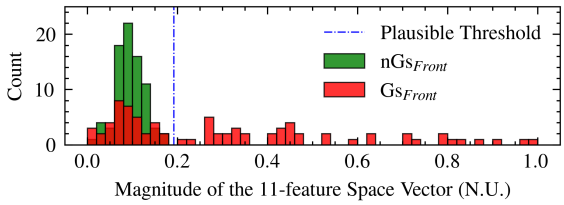

Fig. 4. Distribution based on the magnitude of the 11-feature space vector for the two classes Gs (red) and nGs (green) based on measurements pertaining to varying conditions of when the mannequin is facing toward the DAA. A plausible threshold value of approximately 0.2 N.U. for the magnitude of the 11-feature space vector is observed and shown in dash-dot blue that can separate the two classes. Gs: gun-shape. nGs: non-gun-shape. DAA: dynamic antenna array. N.U.: normalized unit.

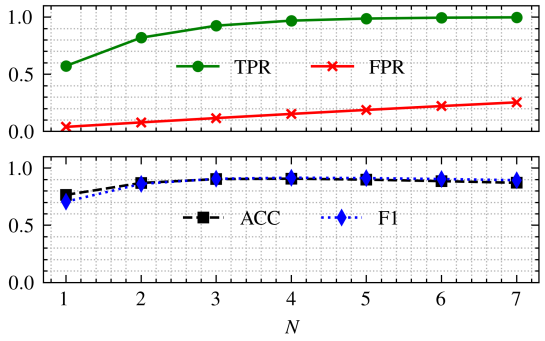

Fig. 5. Classification results using N consecutive independent ring filtered responses of the same scene type. TPR: true positive rate. FPR: false positive rate. ACC: accuracy. $F1$: $F1$-score.

TABLE I
CLASSIFICATION RESULTS SUMMARY OF FIG. 5

N	1	2	3	4	5	6	7
TPR	0.574	0.820	0.925	0.969	0.987	0.995	0.998
FPR	0.041	0.080	0.118	0.154	0.189	0.223	0.255
ACC	0.766	0.870	0.904	**0.908**	0.899	0.886	0.872
F1	0.707	0.862	0.907	**0.916**	0.913	0.905	0.895

We investigated the multicollinearity among the 11 features via principal component analysis (PCA) and determined that the first two principal components contribute 89.1% and 8.6% of the variance between the two classes, respectively, and all 11 features are highly correlated with the first principal component. We note that more complex processing techniques may be used to efficiently extract features and/or implemented to enable other classification approaches. Nevertheless, we performed a Monte Carlo analysis of 10 000 iterations using the simple threshold method based on the heuristically defined features. Each iteration used a randomly selected 70% of the data set for training and the remaining 30% for testing. Under the assumption that individual measurements are independent of each other, we performed classification based on N consecutive measurements of the same scene type for $N = [1, 7]$ where $N = 1$ and $N = 7$ represent classifying a single response and seven consecutive responses, respectively. The averaged classification metrics from the Monte Carlo simulations are shown in Fig. 5 and summarized in Table I. It can be seen that the true positive rate (TPR) improves as N increases but at the cost of increasing false positive rate (FPR). Furthermore, we note that the accuracy (ACC) and $F1$-score ($F1$) peak when $N = 4$ at 0.908 and 0.916, respectively.

The overall screening time for a measurement (i.e., $N = 1$) is less than 1 s assuming the dynamic antenna array can support a rotational speed of 150 revolution per minute (r/min) to accommodate the measurement time of 0.2 s and a

Authorized licensed use limited to: Michigan State University. Downloaded on June 27,2024 at 04:23:30 UTC from IEEE Xplore. Restrictions apply.

processing time of no more than 0.8 s. Given that the dynamic antenna array can theoretically continue to rotate without reset, and since the visibility is symmetric, the scenario of $N = 4$ corresponds to two complete array rotations (i.e., four 180° measurements). We note the increase in overall screening time can be reduced by considering the trade-off between dwell time and system sensitivity, or by improving the processing efficiency. These results indicate that classification of scenes with and without contraband can be supported without the need to form images, and in a time that is commensurate with real-time operation.

IV. Conclusion

We experimentally demonstrated a privacy-preserving contraband detection technique using a 75 GHz dynamic antenna array system. Using commercially available components and simple arithmetic statistical feature extraction, both classification accuracy and $F1$-score above 0.9 were obtained. Furthermore, the collected Fourier responses are not sufficient to form imagery of the screened subject, thus ensuring privacy. These results validate prior predictions on the application of real-time imageless contraband detection and may prove useful for incorporating identification of a wider range of objects when pairing with more complex feature extraction techniques and machine learning-based classifiers.

References

[1] N. Currie and C. Brown, *Principles and Applications of Millimeter-Wave Radar*. Norwood, MA, USA: Artech House, 1987.

[2] J. A. Nanzer, *Microwave and Millimeter-Wave Remote Sensing for Security Applications*. Norwood, MA, USA: Artech House, 2012.

[3] Y. Álvarez, Y. Rodriguez-Vaqueiro, B. Gonzalez-Valdes, F. Las-Heras, and A. García-Pino, "Fourier-based imaging for subsampled multistatic arrays," *IEEE Trans. Antennas Propag.*, vol. 64, no. 6, pp. 2557–2562, Jun. 2016.

[4] E. Kpre, C. Decroze, M. Mouhamadou, and T. Fromenteze, "Computational imaging for compressive synthetic aperture interferometric radiometer," *IEEE Trans. Antennas Propag.*, vol. 66, no. 10, pp. 5546–5557, Oct. 2018.

[5] S. Stanko et al., "Active and passive mm-Wave imaging for concealed weapon detection and surveillance," in *Proc. 33rd Int. Conf. Infr., Millim. Terahertz Waves*, Sep. 2008, pp. 1–2.

[6] D. Chen, S. Vakalis, and J. A. Nanzer, "A 75-GHz dynamic antenna array for real-time imageless object detection via Fourier domain filtering," in *IEEE MTT-S Int. Microw. Symp. Dig.*, Jun. 2022, pp. 727–730.

[7] S. Vakalis, S. Mghabghab, and J. A. Nanzer, "Fourier domain millimeter-wave imaging using noncooperative 5G communications signals," *IEEE Trans. Antennas Propag.*, vol. 70, no. 10, pp. 8872–8882, Oct. 2022.

[8] M. Born and E. Wolf, *Principles of Optics*. Cambridge, U.K.: Cambridge Univ. Press, 1999.

[9] A. R. Thompson, J. M. Moran, and G. W. Swenson, *Interferometry and Synthesis in Radio Astronomy*. Hoboken, NJ, USA: Wiley, 2001.

Authorized licensed use limited to: Michigan State University. Downloaded on June 27,2024 at 04:23:30 UTC from IEEE Xplore. Restrictions apply.